Acta metall. mater. Vol. 38, No. 6, pp. 1163–1174, 1990
Printed in Great Britain.

0956-7151/90 $3.00 + 0.00

MARTENSITIC GROWTH IN ZrO_2—AN *IN SITU*, SMALL PARTICLE, TEM STUDY OF A SINGLE-INTERFACE TRANSFORMATION

Y-H. CHIAO† and I-WEI CHEN

Department of Materials Science and Engineering, University of Michigan, Ann Arbor, MI 48109-2136, U.S.A.

(*Received* 4 *August* 1989)

Abstract—An *in situ* TEM experiment on martensitic growth was performed using submicron ZrO_2 particles of a square-platelet shape. The transformation was between the orthorhombic and the monoclinic phases and involved a simple shear plus a dilatation in the shear plane. The o/m interface propagated at a speed of 2 nm/s, while maintaining a sharp habit plane which was stepped on the unit cell scale. The average inclination of this stepped interface obeyed the invariant plane strain condition. While no long-range stresses were present, dislocation-like line contrast was revealed at the steps. These results are analyzed in terms of the coherency dislocation concept. Fundamental properties, such as the interfacial energy, Peierls stress and nucleus size, have been deduced.

Résumé—Une expérience par MET *in situ* de croissance martensitique est effectuée en utilisant des particules de ZrO_2 submicroniques en forme de plaquettes carrées. La transformation s'effectue entre les phases orthorhombique et monoclinique; elle implique un cisaillement simple et une dilatation du plan de cisaillement. L'interface orthorhombique/monoclinique se propage à la vitesse de 2 nm/s, tandis que se maintient un plan d'accolement net, présentant des facettes à l'échelle de la maille. L'inclinaison moyenne de cette interface en escalier obéit à la condition de déformation plane invariante. Lorsqu'il n'y a pas de contraintes à longue distance, un contraste de lignes, semblable à celui des dislocations, est visible sur les marches. Ces résultats sont analysés d'après le concept des dislocations de cohérence. On en déduit des propriétés fondamentales, telles que l'énergie interfaciale, la contrainte de Peierls et la taille des germes.

Zusammenfassung—Das martensitische Wachstum wurde in submikron-großen ZrO_2-Teilchen in Form quadratischer Plättchen *in situ* im Durchstrahlungselektronenmikroskop untersucht. Die Umwandlung lief zwischen der orthorhombischen und der monoklinen Phase ab und umfaßte eine einfache Scherung und eine Dilatation in der Scherungsebene. Die o/m-Grenzfläche wanderte mit einer Geschwindigkeit von 2 nm/s, dabei blieb die Habitebene scharf mit Stufen in der Größe der Gitterzelle. Die mittlere Neigung dieser gestuften Grenzfläche befolgte die Bedingung invarianter ebener Dehnung. Weitreichende Spannungen traten nicht auf, allerdings fanden sich versetzungsartige Kontraste an den Stufen. Diese Beobachtungen werden anhand des Konzeptes der Kohärenzversetzungen analysiert. Grundlegende Größen, wie Grenzflächenenergie, Peierls-Spannung und Größe des Keimes, werden abgeleitet.

1. INTRODUCTION

Direct microscopic observations of martensitic transformations are rare. In a previous paper [1] by the present authors, *in situ* transmission electron microscopy (TEM) experiments were reported on the martensitic nucleation of the tetragonal (t) to monoclinic (m) transformation ZrO_2. These experiments used small tetragonal ZrO_2 single crystals of the size of 0.2 μm, which were isolated and defect-free. By introducing heterogeneities into these perfect crystals, we could trigger spontaneous transformation in individual particles when the stress amplitudes of the heterogeneities exceeded a critical value. Further qualitative analyses of these results found them in close agreement with the classical nucleation picture for heterogeneous martensitic transformation. Unfortunately, since the t to m transformation in ZrO_2 at room temperature is strongly over-driven by a very large driving force, the transformation is spontaneous and not suitable for detailed studies on the growth process. We now report a parallel study on a geometrically similar martensitic transformation, from orthorhombic (o) to monoclinic ZrO_2, which is weakly driven at room temperature and can be closely monitored, using *in situ* TEM techniques, during the entire growth process. In particular, we have recorded high resolution images of the growth interface at various stages to aid interpretations of the growth mechanism.

Three polymorphs, cubic (c), tetragonal and monoclinic, are well known for ZrO_2 [2]. Among

†Present address: Dow Chemical Central Research, Advanced Ceramics Laboratory, Midland, MI 48674, U.S.A.

them, the monoclinic phase belongs to the space group $P2_1/c$, with lattice parameters $a_m = 0.515$ nm, $b_m = 0.521$ nm, $c_m = 0.531$ nm and an angle $\beta_m = 99.25°$. Several orthorhombic phases have also been reported [3–21], some of them were thought to exist only under a high pressure [3–10] or in a thin foil [11–17]. We have carried out a detailed crystallographic analysis of the orthorhombic phase encountered in our study, using selected area diffraction (SAD) and convergent beam electron diffraction (CBED) techniques, and found that the specific polymorph we studied belonged to the space group Pbca, with lattice parameters $a_o = 1.014$ nm, $b_o = 0.521$ nm and $c_o = 0.511$ nm. (The above analysis and a structural model of the orthorhombic phase will be published elsewhere.) Using the above data and the appropriate lattice correspondence between the two phases, the o to m transformation can be quite accurately described by a simple shear transformation plus a dilatation along one of the in-plane axes on the shear plane, in a way very similar to the t to m transformation [1, 2, 22]. Such transformations may be regarded as a prototype of the simplest, yet nontrivial, class of shear-dominated dilatant martensitic transformations in a crystallographic sense. This simplicity proved to be essential to the observed structure of the growth interface, which was fully coherent.

The invariant plane strain (IPS) condition has been a central concept in the current understanding of martensitic interfaces [23, 24]. The IPS condition, a geometric hypothesis motivated by the considerations of strain energy minimization, demands that the transformation interface takes on a special habit so that no macroscopic distortion or rotation should occur. In cases when the IPS conditions are indeed obeyed, the interfaces determined accordingly are usually crystallographically irrational [23–25]. It would seem more natural, however, to envision the actual atomic interface between two phases to be rational. In this paper we wish to demonstrate, with direct evidence from high resolution images, that a coherent martensitic interface can indeed be constituted of atomically-sharp low-index facets with periodically-spaced lattice steps, which are configured to maintain the IPS habit on a coarser scale. These steps are associated with strain fields characteristic of interface dislocations and they glide in unison as a group in order to effect the planar motion of the transformation interface. It is in this way that the IPS condition manifests itself, structurally and kinematically, as a growth condition for martensitic transformations.

The growth mechanism outlined above is akin to the ledge mechanism in the growth of precipitates [26, 27]. Unlike the latter, however, ledges in martensitic interfaces require no long-range atomic transport for their motion but their structures are strictly constrained by the IPS condition from strain energy considerations. This essential difference gives rise to some different behaviors in ledge structures and kinetics in the two classes of phase transformations, which we will elaborate upon in this paper.

Several investigators in the past have reported observations of martensitic transformations by *in situ* TEM studies [15–17, 28–33]. All of these observations found martensitic plates emanating from some microstructural or micromechanical heterogeneities. Such observations were most commonly made when the driving force was relatively small, just as in the present study. However, since single particle was not used in the previous experiments, the martensitic phase had to be initiated at internal interfaces and grow as a thin plate with two adjacent, and nearly parallel, interfaces under a complicated stress state dictated by the matrix constraint. Martensitic transformation in our small particle experiment, on the other hand, involved only one interface propagating from one side of the particle and was free of any external constraint due to the small size of the crystal. This simplicity made it possible to reveal, *in situ*, and for the first time, the growth interface and the growth steps at the unit cell level.

2. EXPERIMENTAL

The experimental procedure in this study was essentially the same as the one used in Ref. [1]. Submicron sized ZrO_2 particles were prepared by an internal oxidation method. The starting material was a Nb–1%Zr alloy. Cold rolling at room temperature was used to obtain foils of a thickness of 100 μm. They were electropolished by a $HF–HNO_3–H_2SO_4$ solution before heat treatment to obtain clean surfaces. The oxygen partial pressure needed to form ZrO_2 precipitates in the Nb matrix was estimated from the equilibrium-free energy of formation of the oxide [34]. Since the oxygen pressure so determined, 10^{-15} atm, was lower than the dynamic vacuum of the furnace used in the heat treatment, the required oxygen doping was accomplished using the residual atmosphere as the oxygen source. After oxygen doping at 1000°C, the temperature was raised to 1700°C for oxide formation and coarsening. Furnace-cooled specimens were than weighed to determine the weight gain due to the oxygen treatment.

Carbon replica specimens were prepared by a double etching procedure. The first etching exposed ZrO_2 particles to the surface due to the selective etching of the Nb matrix. A thin carbon coating was then evaporated onto the etched surface. Subsequently, the second etching caused the detachment of the carbon layer along with ZrO_2 particles from the specimen surface. The carbon layer was collected using copper TEM grids and found to contain well-separated ZrO_2 particles. Chemical composition of the ZrO_2 particles was inspected by scanning transmission electron microscopy (STEM) X-ray analysis. Since no other metal components than Zr could be identified, the impurity level of the oxide particles was

determined to be below the detection limit of the instrument, *ca* 1% for heavy atoms. 3 mm TEM discs of the Nb–ZrO_2 alloy were also prepared using twin-jet electropolishing. To avoid stressing the metastable oxides, disc specimens were punched out prior to the internal oxidation treatment.

A JEM 200 CX microscope was used in the present work. Most (100) lattice fringe imaging of thin particles was obtained using central illumination with an objective aperture of a size which excludes diffraction spots with interplanar spacing less than 0.25 nm. For *in situ* photography of the moving interface, we found a high speed TEM plate, such as Kodak S0-163, in combination with a bright illumination afforded by the LaB_6 filament in the microscope, was essential. Sharp frozen-in, under-exposed pictures were obtained first. Prolonged developing afterwards was then utilized to compensate the original under-exposure.

3. EXPERIMENTAL RESULTS

3.1. Particle morphology

ZrO_2 particles of interest to the present study were plate-like particles of a roughly square shape. They were tetragonal single crystals when retained in the Nb matrix, but later transformed into orthorhombic phase during preparation of the carbon-supported specimens. Some of them remained tetragonal even at this stage, then transformed into orthorhombic ones during examination in the microscope. More rounded particles were found to remain mostly tetragonal, so they were used in the nucleation experiments on the t to m transformation which we already reported [1].

Bounding surfaces of the square, plate-like particles were of the {100} type. A Bain orientation relationship between the ZrO_2 particles and the Nb matrix, $(110)_{Nb} \| (200)_{t\text{-}ZrO_2}$ and $[001]_{Nb} \| [001]_{t\text{-}ZrO_2}$, existed between the two, as shown in Fig. 1. We found that Moiré fringes formed between two lattice spacings, $d_1 = 0.234$ nm of $(100)_{Nb}$ and $d_2 = 0.254$ nm of $(200)_{t\text{-}ZrO_2}$ [or $d_2 = 0.260$ nm of $(002)_{t\text{-}ZrO_2}$], provided very useful information. From the identical spacing of Moiré fringes, $d_1 d_2/(d_2 - d_1) = 2.90$ nm in Fig. 1(a, b), we concluded that the platelet lied on $(001)_{t\text{-}ZrO_2}$ and was bounded by crystallographically equivalent $(100)_t$ and $(010)_t$ planes. A side view further confirmed the platelet morphology. A width/thickness aspect ratio of 4 was also determined.

As mentioned above, these tetragonal particles often transformed into orthorhombic ones when removed from the Nb matrix. Using SAD and CBED, we found the transformation followed lattice correspondence (LC) B, i.e. $(010)_o \| (001)_t$, $[100]_o \| [100]_t$. Recalling that the lattice parameters of the orthorhombic phase, a_o, b_o and c_o, are 1.014, 0.521 and 0.511 nm, respectively, and those of the tetragonal phase, a_t and c_t, are 0.509 and 0.519 m, respectively, it is obvious that the (LC) B can maintain a close matching between b_o and c_t. This seems to be the reason why the lattice correspondence was favored.

3.2. In situ characterization of o–m transformation

Initiation of o to m transformation was achieved by focusing a 200 kV electron beam onto an orthorhombic particle. An $[010]_o$ view of the particle revealed that the transformation was nucleated from one of the four corners of the square platelet. In Fig. 2 we present a series of frozen-in images of a transforming particle. Figure 2(a) is a set of double exposure images taken at 10 s apart showing the transformation interface moved from position 1 to position 2 at a speed of 2 nm/s. Figure 2(b) shows the interface, viewed edge-on, at a 13° inclination from $(100)_o$. The transformed portion of the particle had a shape change of a simple shear type by 9° toward $[001]_o$ on $(100)_o$. The total shape change, when the entire particle is transformed, is made clear by Fig. 2(c).

Diffraction analysis of partially transformed particles allowed a positive identification of the monoclinic phase and the o/m orientation relationship. Figure 3 shows an indexed pattern so obtained: the lattice correspondence is of the type $(100)_o \| (100)_m$ and $[010]_o \| [010]_m$. The shear strain shifts the 002_m spot to an angle $\beta_m = 99.30°$. In addition, a relative dilatation of $(002)_m$ is indicated by the inward shift of the monoclinic spots in that direction. Using this LC and the relative lattice parameters determined from Fig. 3, we obtain directly the approximate transformation strains, $e_{xx} = 0.0056$, $e_{zz} = 0.0393$ and $e_{xz} = 0.0812$, by letting x be $[100]_o$ and z be $[001]_o$. These values may be compared with the transformation shape strains of the t to m transformation, which has a simple shear of 0.0814 and a dilatation of 0.0421 [1, 2, 22]. Geometrically, the two transformations are very similar indeed.

The consequence of the above orientation relationship on transformation habit can be best appreciated by referring to the construction of Fig. 4 in which the transformation shear and dilatation are depicted. An undistorted, unrotated plane, denoted by h, is evident at an inclination of 13.5° to $(100)_o$. This is precisely the habit plane we observed in Fig. 2. Since $e_{xx} = 0$, the IPS condition, which is obviously satisfied by the habit plane, is reduced to the simple requirement of $\theta = \tan^{-1}(e_{zz}/2e_{xz})$ where θ is the inclination. This result is nearly unchanged even if a non-zero but small e_{xx} is considered. This undistorted, unrotated habit plane between the two phases minimizes the strain energy of the system by eliminating the long-range stress field. The latter was verified by a trace analysis from low magnification lattice fringe images of the transforming particle, which showed no lattice fringe distortion during the transformation when the IPS interface was maintained.

3.3. Stepped structure of o/m interface

The o/m interface had an irrational habit orientation close to $(80\bar{1})_o$. As mentioned in the Introduction, it

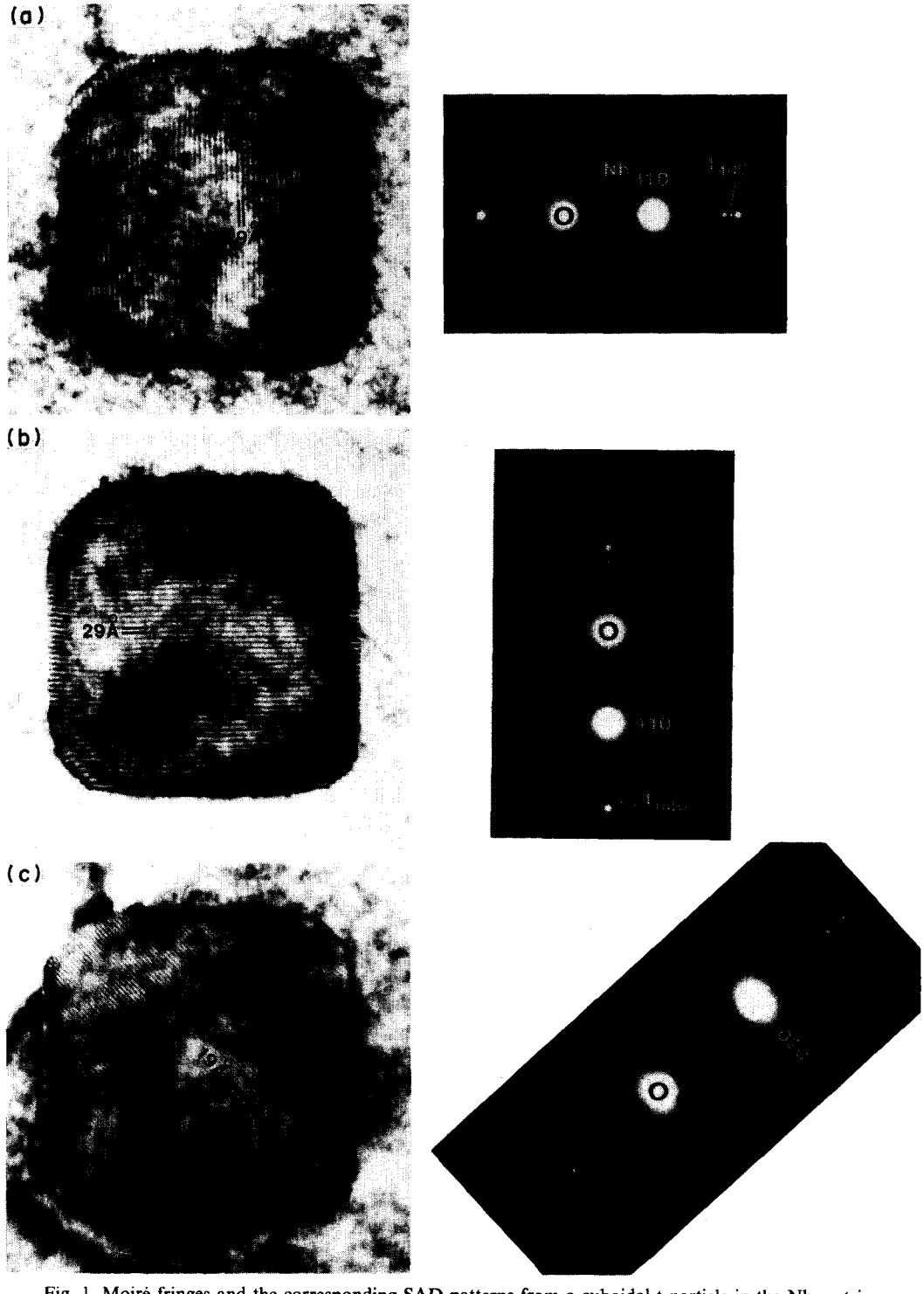

Fig. 1. Moiré fringes and the corresponding SAD patterns from a cuboidal t particle in the Nb matrix. Spacing between the Moiré fringes and the missing of odd ordered spots in the diffraction pattern confirm the t symmetry. The parallelism of diffraction spots along three different directions indicates a Bain orientation relationship described in the text.

seems reasonable to expect an irrational plane to be composed of rational, faceted planes with periodic lattice steps between them. In order to lend support to the above speculation, high magnification lattice fringe imaging was attempted in the *in situ* experiment. Figure 5 shows the (100) lattice image so obtained. Two sets of lattice fringe spacings can be resolved, the one with the 1.0 nm spacing defines the untransformed orthorhombic region whereas the one with the 0.5 nm spacing covers the transformed

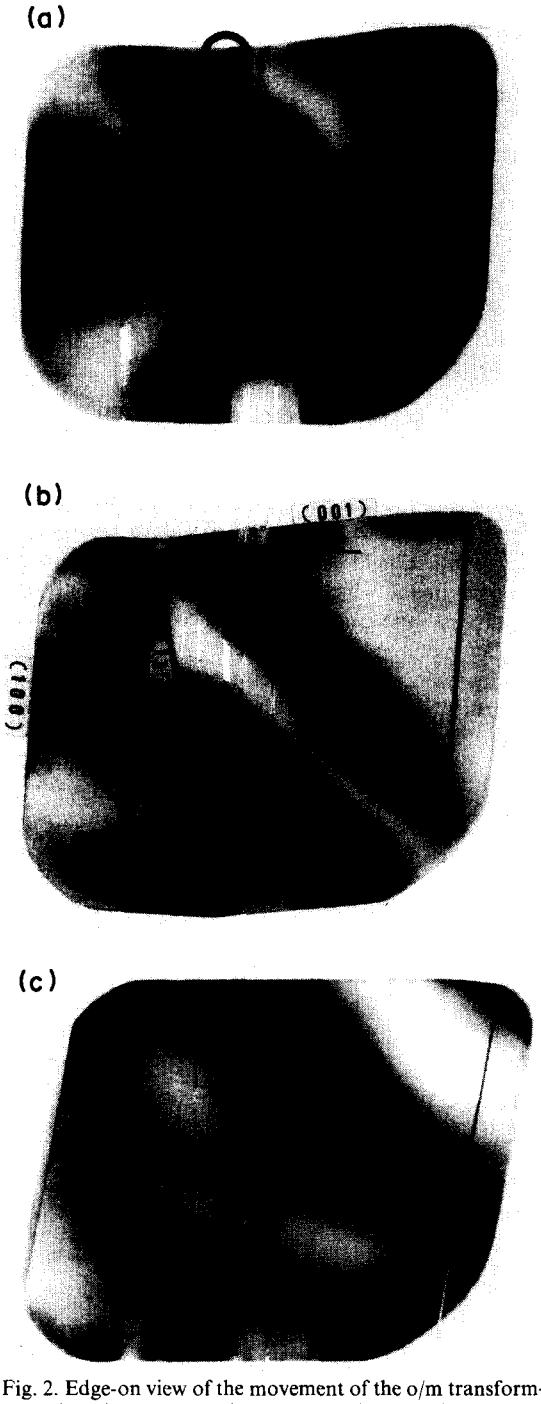

Fig. 2. Edge-on view of the movement of the o/m transformation interface. (a) Double exposure image taken at 10 s apart. A local deviation of the interface orientation from IPS, marked by the circle, forms a stress center. (b) Viewed at a later time. The transformation interface is inclined from (100) by 13°. Transformed portion of the particle undergoes a 9° simple shear on (1,0,0). (c) Transformation completed.

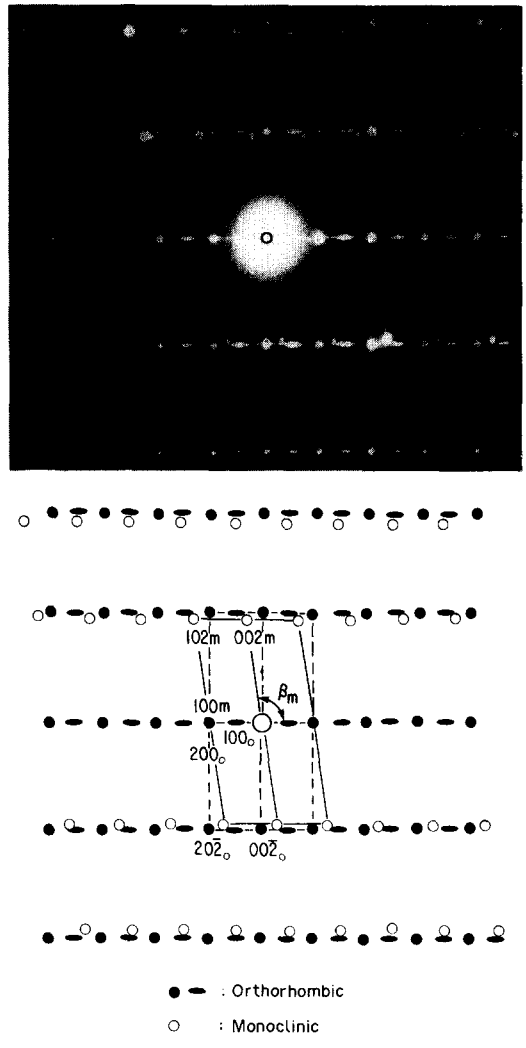

Fig. 3. SAD pattern from a partially transformed particle indicating the orientation relationship and the transformation strains.

monoclinic region. The two sets of lattice fringes are parallel to each other, thus confirming directly the $(100)_o \| (100)_m$ orientation relationship deduced previously from the diffraction pattern. As expected, the transformation interface has a stepped structure. The faceted plane is (100). The step height is exactly one interplanar spacing of $(100)_o$ planes, i.e. 1.0 nm. The steps are periodically spaced at 4.2 nm apart. This periodic spacing is just what is required because the ratio of step-height/step-spacing should be tan 13.5°.

As mentioned before, the interface velocity was 2 nm/s. This velocity is denoted as v_1. If we envision the interface movement to be accomplished by a lateral movement of lattice steps, at a velocity v_2 from left to right in Fig. 5, then $v_1/v_2 = \tan(13.5°)$, giving $v_2 = 8.3$ nm/s. Knowing the exposure time for Fig. 5, we have computed the distance of step movement during imaging, 2.3 nm, and marked it as δx on the upper right margin of Fig. 5. Such movement caused a blurred contrast over a distance δx around each step and this effect is clearly noticeable in Fig. 5.

3.4. *Transformation dislocations*

We have attempted an alternative approach to resolve the short-range stresses associated with the stepped IPS interface. The idea behind this approach

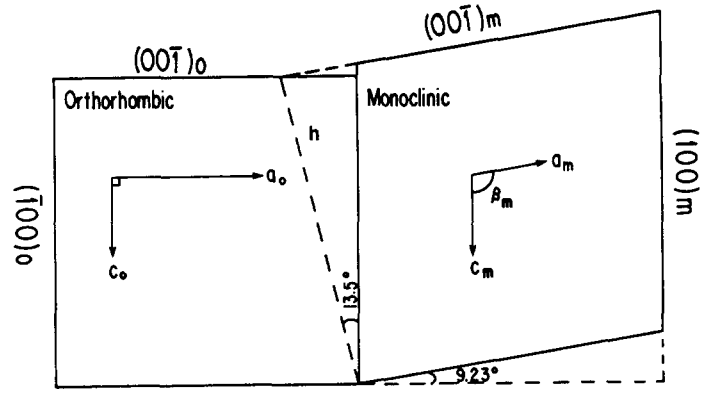

Fig. 4. Schematic of the IPS condition accommodating a linear dilatation and a simple shear. The IPS interface is indicated as h.

originated from the coherency dislocation model of Olson and Cohen [35, 36], which is depicted in Fig. 6. Using this picture, the shear and dilatation components of the transformation can be decomposed and naturally associated to a set of interface dislocations on the two parts of the bifurcated interface. Thus, interface structure should have strain fields characteristic of dislocations which can be revealed by TEM under the appropriate imaging conditions.

For the shear component, it is clear from Fig. 6 that, along the step vector, the lattice vector in the a direction undergoes a lattice shear deformation of $\tan(\beta_m - 90°)$, from a_o to a_m. This component can be formally described by a set of transformation dislocations situated at the steps, with a Burgers vector $b_2 = (0, 0, 0.165)$ in units of nm. (Transformation dislocations of the above type are entirely analogous to the so-called twinning dislocations used to describe a coherent twin interface [37–39].) Similarly, for the dilatation component, it is clear from Fig. 6 that along the (100) plane, the lattice vector in the c direction undergoes a lattice dilatation of 0.039, from c_o to c_m. This component can be formally described by a set of misfit dislocations situated at every lattice point on the (001) planes, with a Burgers vector $b_1 = (0,0,0.020)$ in units of nm. (Transformation dislocations of the latter type are entirely analogous to the so-called surface dislocations used to describe an inclusion/matrix interface [39–41].)

To reveal transformation dislocations b_2, we attempted *in situ* diffraction contrast imaging. At the (002) systematic diffraction condition, after tilting the moving interface to an inclined orientation around [002], a bright field image was obtained. Figure 7 shows the image which reveals an array of contrast lines across the inclined interface. The average periodicity of the contrast lines is 4.2 nm, which is consistent with the step spacing found in Fig. 5 but significantly different from the expected Moiré fringe spacing between (002) spots of the two phases. Thus, the line features observed were thought to be due to a dislocation contrast. Consistent with the present imaging condition, the contrast also implies that the Burgers vector has an appreciable component along [001], again consistent with dislocations b_2. Unfortunately, with a moving interface, there was not

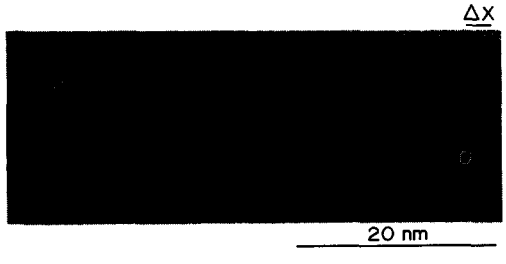

Fig. 5. (1,0,0) lattice fringe image of an edge-on o/m transformation interface showing a stepped structure on the unit cell level.

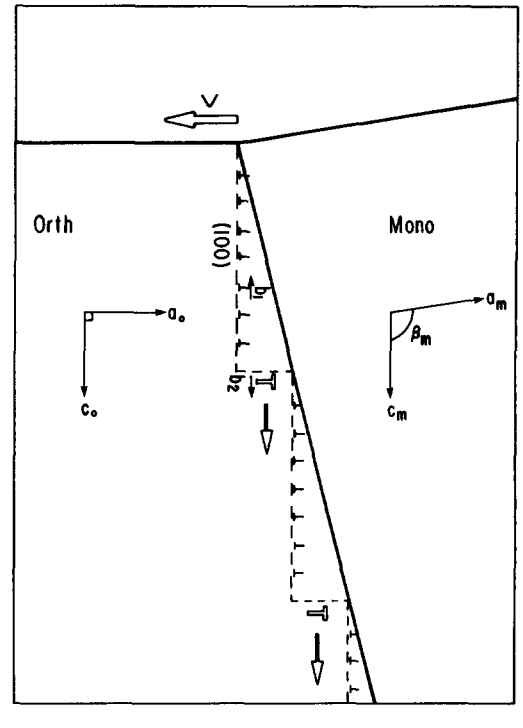

Fig. 6. Schematic of the coherency dislocation structure of the o/m interface. The net vector sum of Bergers vectors is zero.

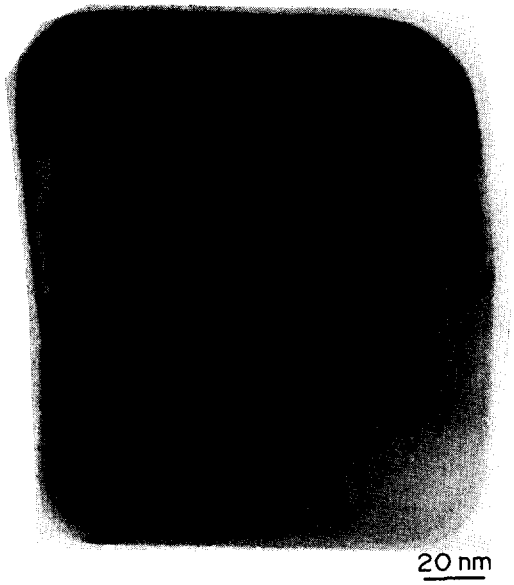

Fig. 7. Bright field image of an inclined o/m transformation interface taken at a [1,0,0] systematic diffraction orientation. The fringes along the interface at an average spacing of 4.3 nm are line contrasts due to a nonvanishing g·b component.

sufficient time in our experiment to perform a more detailed Burgers vector analysis.

Dislocations b_1, which are located on every (001) plane, do not have a sufficiently localized line contrast themselves. In this sense, their dislocation character is not well defined. Indeed, they may be regarded as a continuous distribution of "virtual" dislocations along the interface as described in the surface dislocation picture [39–42]. Nevertheless, a broad periodic strain contrast, which is probably due to the misfit of type b_1, can be discerned between steps in Fig. 5.

The line contrast of Fig. 7 was observed to shift slowly toward the right as the o/m interface moved downward. This can also be interpreted by the picture of Fig. 6 which shows that during phase transformation, dislocations b_2 glide along [001], while dislocations b_1 climb *conservatively* along [100]. The cooperative movement of these two sets of dislocations results in the propagation of the stepped interface. Thus, the dislocation picture of the transformation interface not only is meaningful for understanding the strain fields, but is also useful for understanding interface kinetics. We will return to the latter point in the Discussion.

3.5. Impingement of transformation variants

The cuboidal, plate-like geometry of the orthorhombic particle studied here permitted a certain probability of multiple nucleation events at more than one corner during the lifetime of o to m transformation. Two distinguishable cases are schematically depicted in Fig. 8 for two successive nucleation events. If nucleation occurs at two diagonal-sharing corners, it leads to mutual annihilation of the two o/m interfaces and the final m particle is still a single crystal. This was observed experimentally as shown by the serial micrographs [Fig. 9(a–d)]. Note that the monoclinic variant marked as 2 in Fig. 9(a) had already assumed the habit orientation, even though it was only six or so unit cell layers in thickness at that point. (There are two dark contrast bands running vertically across the particle in Fig. 9. Their origin had been traced to stacking faults in the orthorhombic phase as described elsewhere.) On the other hand, if nucleation occurs at two edge-sharing corners, it leads to the impingement of the two monoclinic variants, creating a twin interface. This was observed

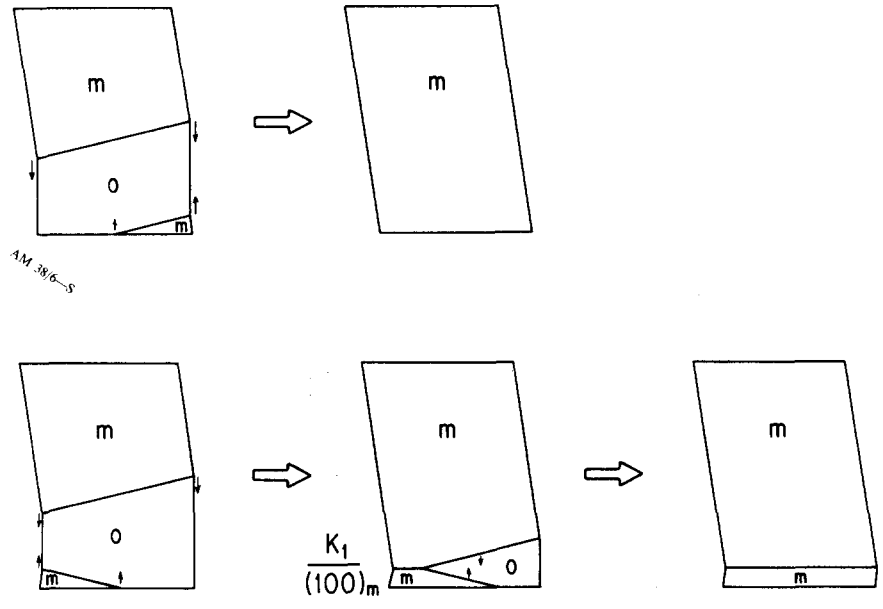

Fig. 8. Schematic of two possible events leading to impingement of the m variants.

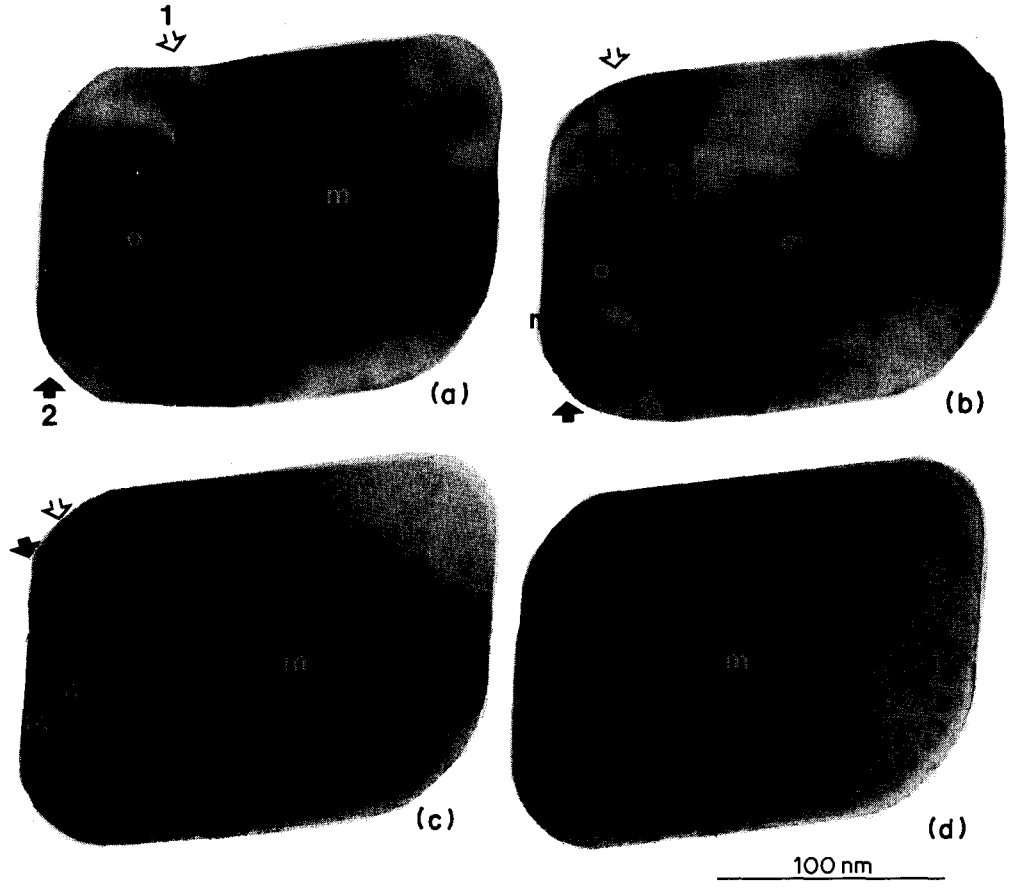

Fig. 9. An edge-on view of the coalescence of two parallel o/m transformation interfaces from two opposite corners. The variant initiated from the lower left corner of (a) has already assumed the IPS habit.

experimentally, as shown in Fig. 10, under the (100) lattice fringe imaging condition. As impingement proceeded, the two opposing o/m interfaces zippered up to form a twin plane, pinching off the remaining orthorhombic triangle. (In the terminology commonly used for twinning, the twin interface here is of the so-called K_1 type [43].) It is again remarkable to note that the transformation interfaces continued to maintain their characteristic habit orientations and step structures down to the last few unit cell layers [e.g. three in Fig. 10(b)].

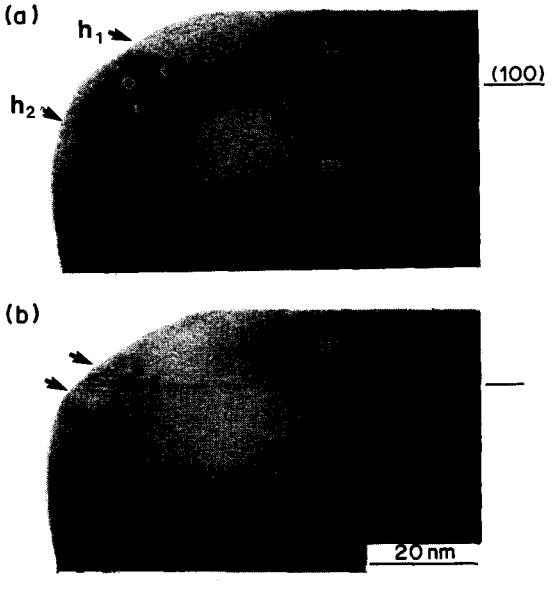

Fig. 10. (1,0,0) twin related variants formed by the coalescence of two symmetrically oriented o/m transformation interfaces. The two IPS interfaces remain faceted until the very end.

4. DISCUSSION

4.1. The o to m transformation

Based on the experimental observations summarized in the previous section, the following picture of single-interface martensitic growth in ZrO_2 single crystals emerges. The monoclinic phase first nucleated at a corner, and its interface with the orthorhombic phase assumed an IPS habit at a very early stage and throughout the span of the phase transformation. This interface remained coherent by bifurcating into alternating (100) planes and lattice steps of

one unit cell height, at a periodicity of 4.2 nm. There was no long-range stress field in either phase during the transformation. However, some short-range, edge dislocation-like strains were associated with the steps; in addition, smaller misfit strains remained with the (100) interface. The interface propagated by the cooperative movement of all the steps in the [001] direction, which was formally equivalent to the glide of the transformation dislocations associated with the steps. During the above process, new steps were periodically nucleated at the free surface and they later exited at the opposite free surface.

The structural picture of the transformation interface, in terms of transformation and misfit dislocations, offers a particularly convenient way to assess several basic quantities relevant to the mechanism of martensitic transformation.

4.2. *Interfacial energy*

The dominant contribution to the interfacial energy probably comes from the elastic energy associated with the short range stresses near the interface. These stresses arise because of the local deviation from the IPS condition and can be attributed to two sets of interfacial dislocations b_1 and b_2. The net vector sum of Burgers vectors along the (100) facet and the step, of course, should be zero to ensure that all long-range stresses would vanish. This can be directly verified by noting that the spacing between b_2 was about eight times that between b_1, and that $b_2 + 8b_1 \approx 0$. The interfacial energy can then be computed by summing up the self energies of interfacial dislocations over a short range only.

The dislocation self-energy is given by the following equation [43]

$$E = [\mu b^2/4\pi(1-\nu)]\ln(R\alpha/b). \tag{1}$$

In the above, μ is the shear modulus, ν is the Poisson's ratio, b is the Burgers vector, R is the cut-off radius and α is a numerical constant. Since the dislocation self-energy scales with b^2 and $b_2 \gg b_1$, it follows that it is b_2, i.e. the transformation dislocation at the step, that is responsible for most of the strain energy. At a distance beyond approximately the half spacing of the steps, L, however, the stress field due to b_2 is cancelled by those of misfit dislocations b_1. Hence, we let $R = L/2$. From the above considerations, the interfacial energy due to dislocations b_2 at a spacing L may be written as

$$\gamma = [\mu b_2^2/4\pi(1-\nu)L]\ln(L\alpha/2b_2). \tag{2}$$

For estimation, values of μ and ν of tetragonal and cubic zirconia, $\mu = 80$GPA and $\nu = 0.3$, are adopted here [44]. The numerical constant α is taken as 3, typical for ionic crystals [43]. From our experiment, $b_2 = 0.165$ nm and $L = 4.2$ nm. Substituting these quantities into equation (2), we estimate the interfacial energy as $0.15\ \mathrm{J/m^2}$.

The above estimate of interfacial energy is close to the one (i.e. $0.2\ \mathrm{J/m^2}$) we adopted in the past for the analysis of nucleation experiments on the t to m transformation [1, 22]. It is also similar in magnitude to the interfacial energy between cubic and tetragonal zirconia as inferred from precipitate coarsening experiments (i.e. 0.1–$0.2\ \mathrm{J/m^2}$) [45].

4.3. *Interfacial friction*

Our experiments found that the interface propagated at a constant speed during the phase transformation, which was much less than the limit of the sound speed. Since the interface was driven by a chemical driving force, the above observation indicated that there was a friction on the motion of the interface that just balanced the driving force. Inasmuch as the interface may be regarded as to contain a set of interface dislocations, the origin of the friction can be attributed to the glide resistance on the transformation. More specifically, indeed, we may identify the Peierls stress to be responsible for the glide resistance. This seems reasonable because no obstacle to the interface was visible in the single crystals studied here and no external mechanical stress or matrix constraint was present in our experiment. The Peierls stress reflects the fact that the energy of the dislocation, and the interface as well, fluctuates with the position; the amplitude and wavelength of the fluctuation are determined by the strength and separation of the interionic bonds. In the literature of martensitic transformation, Cohen and Kaufman had called attention to such friction and envisioned them as "grass on the hill" which manifested itself as a friction on the martensitic interface [46]. Some evidence already exists on the possible role of such friction in martensitic nucleation and growth [47, 48] although in metallic alloys, the Peierls stress tends to be overshadowed by dislocation interactions with solute atoms, defect clusters and other dislocations [47–50]. In contrast, single-phase pure oxides such as ZrO_2, in which the Peierls stress tends to be predominant in controlling dislocation mobility, should provide a more promising case to test the lattice friction. In the following we attempt to obtain a direct estimation of the Peierls stress in our experiment.

Denoting the chemical driving force per unit volume as g_{ch}, and the glide resistance as τ_p, then the glide force on the dislocation b_2 is $g_{ch}H$ per unit length, where H is the step height and the counteracting lattice friction is $\tau_p b_2$. Since the glide resistance decreases rapidly with the Burgers vector and the friction is additionally proportional to b, only the friction on the transformation dislocations b_2, but not b_1, need to be considered. At the steady state, force equilibrium requires that

$$\tau_p = g_{ch}H/b_2. \tag{3}$$

The chemical driving force of the o to m transformation can be estimated from the recently published pressure (P)–temperature (T) phase diagram of the tetragonal, orthorhombic, and monoclinic phases for

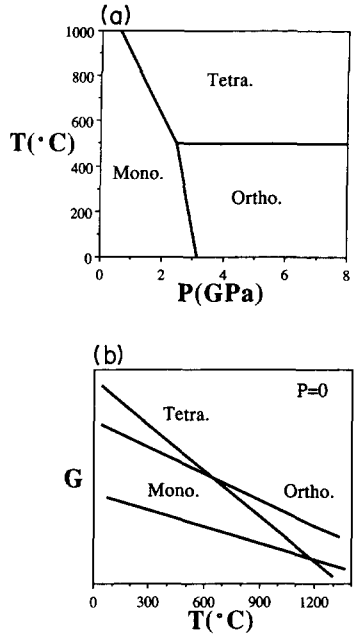

Fig. 11. (a) P–T phase diagram of ZrO_2. (b) Schematic free energy diagram at $P = 0$.

ZrO_2 [10, 51], which is sketched in Fig. 11(a). (Orthorhombic phase probably has several polytypes of a similar phase stability but different stacking sequence and symmetry. The orthorhombic phase reported for the P–T diagram appears to be different from the phase we studied here only in the above sense.) Note that the o/t phase boundary extrapolates at lower pressures to an o/t equilibrium temperature of 500°C at $P = 0$. Using the Clausius–Clapeyron equation and the volume difference between o and m phase, the entropy of the o to m transformation can be estimated from the slope of the P–T boundary between o and m phases to be 1.67 J/mol K or 8.28×10^4 J/m^3 K. It is also well known that the entropy of the t to m transformation, with an equilibrium temperature of 1150°C, is 4.18 J/mol K or 2.07×10^5 J/m^3 K. Using these data and a linear approximation for the Gibbs free energies, we have constructed a schematic free energy diagram at $P = 0$, as shown in Fig. 11(b), for the three phases. The driving force of the o to m transformation at 20°C is then estimated as $g_{ch} = 1.7 \times 10^8$ J/m^3, to be compared with 2.3×10^8 J/m^3 in the case of the t to m transformation. Substituting this value and $H = 1.014$ nm into equation (3), the glide resistance τ_p on b_2 is estimated to be 1.0 GPa or $1.2 \times 10^{-2}\,\mu$.

The glide resistance for perfect edge dislocations at 0 K can be estimated from the recent data of compressive yield of Lankford *et al.* on a number of single and polycrystalline zirconia, as 1.5 GPa at room temperature [52]. This value is reasonably close to the value of $2.0 \times 10^{-2}\,\mu$ suggested by Frost and Ashby [53] for UO_2 and ThO_2, which have a structure similar to ZrO_2. Since b_2 dislocations have a smaller Burgers vector (0.165 nm) than that of the perfect 1/2⟨110⟩{001} dislocation (0.359 nm), a smaller Peierls stress on b_2 as estimated above seems quite reasonable.

At finite temperatures nucleation of kink-pairs, which subsequently spread apart, may lower the Peierls stress somewhat and introduce a thermally-activated component to it. This process may be described by an activation volume which should be characteristically small, of the order of a few b^3, if the double-kink mechanism is operational. Indeed, measurements of rate dependence and stress relaxation of transformation plasticity in zirconia ceramics have provided some indication that such a mechanism may be operating in this class of ceramics [54, 55].

4.4. *Nucleation of the monoclinic phase*

It was evident from the present experiment that the monoclinic phase was nucleated at the corners of the square, plate-like particle. Evidence from Fig. 9(a) further indicated that the habit plane was adopted at a very early stage of the transformation. [The monoclinic phase at the lower left corner of Fig. 9(a) was only six unit cells thick at its thickest end.] If the IPS condition was also obeyed at the nucleation stage, then the configuration of the critical nucleus can be evaluated as follows.

The monoclinic nucleus formed at a corner has a wedge-like shape initially, before the o/m interface is fully extended to the two opposite sides of the plate. The total o/m interfacial area increases as the nucleus grows at this stage. Let the length of the monoclinic wedge be l and the width be w, then the free energy of the wedge-like nucleus is

$$\Delta G = -g_{ch} lw/2 + \gamma(l^2 + w^2)^{1/2}. \qquad (4)$$

Since $w/l = \tan 13.5°$, we can determine the condition for the critical nucleus in terms of the coordinate w. It gives the width of the critical nucleus as

$$w^* = \gamma/\Delta g_{ch} \cos(13.5°).$$

Using $\gamma = 0.15$ J/m^2 and $g_{ch} = 1.7 \times 10^8$ J/m^3 as before, we estimate the critical nucleus to have a width of 0.9 nm, or slightly less than one unit cell height in the parent phase. This estimation is consistent with our observation that, at a thickness of six unit cells, the habit plane was already propagating steadily and the transformation was well into the growth stage.

5. CONCLUDING REMARKS

A ledge mechanism is also believed to operate in diffusional growth of phases [26, 27]. Growth ledges are needed for the kinetic reason, following the earliest proposal of Gibbs for the growth of close-packed crystal faces into a vapor or liquid matrix [56]. Partially or fully coherent interface boundaries fulfilling the above descriptions can migrate normal to themselves only by first creating a ledge, with the riser

or edge of the ledges being assumed to have a disordered structure. Very likely these ledges contain kinks where interfacial disorder required for ready passage of atoms across the interface and their incorporation into the crystal structure is assured. Kinks and kink migration have been recently observed by *in situ* TEM. [57]. The requirement for a glissile interface in martensitic transformation, which is diffusionless, is quite different. Indeed, a coherent interface such as the one observed in the o to m transformation is always glissile if the driving force is sufficient to overcome the lattice resistance. When lattice invariant deformation [23, 24] is also present and the IPS condition demands a more complex interfacial structure, such as that consisting of one or more sets of lattice or partial dislocations as in the f.c.c. → b.c.c. transformation [39, 50], then the interface is mobile only if all the interface dislocations are glissile.

Although the IPS condition is often obeyed in diffusional transformations [25, 27, 58–60], ledges and kinks reported in the literature tend to be "superledges" and "superkinks" with a step height much larger than the unit cell dimension [26, 27, 57. 61]. In contrast, steps we observed at the o/m interface are of a unit cell dimension. According to the analysis in the previous section, a larger step height will increase the range of interfacial stresses and should cause a much higher interfacial energy. In diffusional transformations, however, some of these stresses could be relaxed by adopting a disordered interfacial structure. thereby permitting superledges and superkinks to exist. The other reason for the difference could be due to the relative difficulty of nucleating ledges and kinks in diffusional phase transformations, such as precipitation, compared to the small particle martensitic experiments of ours. At any rate, it is gratifying to verify that the IPS condition and the ledge mechanism can and does operate at the finest unit cell scale when the situation permits.

Acknowledgements—The small particle experiment was previously described by Y. H. Chiao in his Ph.D. thesis submitted to the Massachusetts Institute of Technology in September, 1986. Our current research on zirconia is supported by the U.S. National Science Foundation, Grant Number DMR-8807024.

REFERENCES

1. I-Wei Chen and Y-H. Chiao, *Acta metall.* **33,** 1827 (1985).
2. E. C. Subbarao, *Adv. Ceram.* **3** (1981).
3. N. A. Bendeliani, S. V. Popova and L. F. Veraschagin, *Geochimya* **6,** 677 (1967).
4. G. Bocquillon, C. Susse and B. Vodar, *Rev. Int. Hautes Temp. Refract.* **5,** 247 (1968).
5. G. Bocquillon and C. Susse, *Rev. Int. Hautes Temp. Refract.* **6,** 263 (1969).
6. L. M. Lityagina, S. S. Kabalkina, T. A. Pashkina and A. I. Khozyainov, *Soviet Phys. Solid St.* **20,** 2009 (1978).
7. H. Arashi and M. Ishigame, *Physica status solidi A* **71,** 313 (1982).
8. L. C. Ming and M. H. Manghnani, in *Solid State Physics under Pressure: Recent Advances with Anvil Devices* (edited by S. Minomura), p. 135. KTK Science, Tokyo (1985).
9. Y. Kudoh, H. Takeda and H. Arashi, *Phys. Chem. Mineral.* **13,** 233 (1986).
10. H. Arashi, O. Shimomura, T. Yagi, S. Akimoto and Y. Kudoh, *Adv. Ceram.* **24,** 493 (1988).
11. A. N. Tyumentsev, A. D. Korotaev, Yu P. Pinzhin, V. Ch. Gonchikov, I. V. Levin, K. A. Markov and S. F. Tyumentseva, *Izv. Vuzov, Fizika* **4,** 40 (1982).
12. L. H. Schoenlein and A. H. Heuer, in *Fracture Mechanics of Ceramics 6* (edited by R. C. Byadt, A. G. Evans, D. P. H. Hasselman and F. F. Lange), p. 309. Plenum, New York (1983).
13. A. H. Heuer, L. H. Schoenlein and S. Farmer, in *Science of Ceramics 12* (edited by P. Vincenzini), p. 257. Ceramurgia s.r.l., Italy (1984).
14. Y-H. Chiao and I-W. Chen, in *Proc. JIMIS-4, Grain Boundary Structure and Related Phenomena, Suppl. Trans. Japan Inst. Metals*, Vol. 27, p. 197 (1985).
15. A. H. Heuer, R. Chaim and V. Lanteri, *Adv. Ceram.* **24,** 3 (1988).
16. B. C. Muddle and R. H. J. Hannink, *Adv. Ceram.* **24,** 89 (1988).
17. T. A. Bielicki, U. Kahmen, G. Thomas and K. H. Westmacott, *Adv. Ceram.* **24,** 485 (1988).
18. R. Suyama, H. Takubo and S. Kume, *J. Am. Ceram. Soc.* **68,** C-237 (1985).
19. R. Suyama, T. Ashida and S. Kume, *J. Am. Ceram. Soc.* **68,** C-314 (1985).
20. O. Ohtaka, S. Kume, T. Iwami and K. Urabe, *J. Am. Ceram. Soc.* **71,** C-164 (1988).
21. D. B. Marshall, M. R. James and J. R, Porter, *J. Am. Ceram. Soc.* In press.
22. I-W. Chen and Y-H. Chiao, *Acta metall.* **31,** 1627 (1983).
23. M. S. Wechsler, D. S. Leiberman and T. A. Read, *Trans. Am. Inst. Min. Engrs* **194,** 1503 (1953).
24. J. S. Bowles and J. K. MacKenzie, *Acta metall.* **2,** 129, 138, 224 (1954).
25. D. S. Lieberman, in *Phase Transformations* (edited by H. I. Aaronson), p. 1. Am. Soc. Metals, Metals Park, Ohio (1970).
26. H. I. Aaronson, C. Laird and K. R., Kinsman, in *Phase Transformations* (edited by H. I. Aaronson), p. 1. Am. Soc. Metals, Metals Park, Ohio (1970).
27. H. I. Aaronson, J. K. Lee and K. C. Russell, in *Precipitation Processes in Solids* (edited by K. C. Russell and H. I. Aaronson), p. 31. F.M.S.-A.I.M.E., Warrendale, Pa (1978).
28. P. L. Ferraglio and K. Mukherjee, *Acta metall.* **22,** 835 (1974).
29. L. Guzman and M. Rühle, in *Proc. ICOMAT-79* (edited by W. S. Owen), p. 590. MIT, Cambridge, Mass. (1979).
30. J. Vanlanduyt, S. Amelinckx, H. VanderHeide, J. P. Sanchez and G. F. Van Bruggen, *Electron Microscopy* **1,** 406 (1980).
31. C. M. Hwang, M. B. Salamon and C. M. Wayman, *Phil. Mag.* **47,** 177 (1983).
32. A. H. Heuer and M. Rühle, *Acta metall.* **33,** 2101 (1985).
33. R-R. Lee and A. H. Heuer, *J. Am. Ceram. Soc.* **71,** 694, 701 (1988).
34. H. Jehn and P. Ortali, *Z. Metall.* **65,** 586 (1974).
35. G. B. Olson and M. Cohen, *Acta metall.* **27,** 1907 (1979).
36. G. B. Olson, *Acta metall.* **29,** 1475 (1981).
37. J. Frenkel and T. Kontorova, *J. Phys. Moscow* **1,** 137 (1939).
38. F. C. Frank and J. H. VanderMerwe, *Proc. R. Soc. A* **198,** 205 (1949).

39. J. W. Christian and K. M. Knowles, in *Proc. Int. Conf. on Solid to Solid Phase Transformations* (edited by H. I. Aaronson, D. E. Laughlin, R. F. Sekerka and C. M. Wayman), p. 1185. T.M.S.-A.I.M.E, Warrendale, Pa (1982).
40. B. A. Bilby, R. Bullough and E. Smith, *Proc. R. Soc. A* **231,** 263 (1955).
41. R. Bullough and B. A. Bilby, *Proc. Phys. Soc.* **69,** 1276 (1956).
42. J. P. Hirth and R. W. Balluffi, *Acta metall.* **21,** 9239 (1973).
43. J. P. Hirth and J. Lothe, *Theory of Dislocations*, 2nd edn. Wiley, New York (1982).
44. I-W. Chen and P. E. Reyes-Morel, *J. Am . Ceram. Soc.* **69,** 181 (1986).
45. J. M. Marder, T. E. Mitchell and A. H. Heuer, *Acta metall.* **31,** 387 (1983).
46. L. Kaufman and M. Cohen, *Prog. Metal Phys.* **7,** 165 (1958).
47. C. L. Magee, in *Phase Transformations*, p. 115. Am. Soc. Metals, Metals Park, Ohio (1970).
48. G. B. Olson and M. Cohen, *Metall. Trans. Am. Soc. Metals* **7A,** 1915 (1976).
49. W. S. Owen, F. J. Schoen and E. R. Srinivasan, in *Phase Transformations* (edited by H. I. Aaronson), p. 157. Am. Soc. Metals, Metals Park, Ohio (1970).
50. G. B. Olson and M. Cohen, in *Dislocation Theory of Martensitic Transformations* (edited by F. R. N. Nabarro), Vol. 17, p. 297. North-Holland, Amsterdam (1986).
51. S. Block, J. A. H. DaJornada and G. J. Piermarini, *J. Am. Ceram. Soc.* **68,** 497 (1985).
52. J. Lankford, R. A. Page and L. Rabenberg, *J. Mater. Sci.* **23,** 4144 (1988).
53. H. J. Frost and M. F. Ashby, *Deformation Map.* Pergamon Press, New York (1983).
54. I-W. Chen and P. E. Reyes-Morel, in *Advanced Structural Ceramics* (edited by P. F. Becher, M. V. Swain and S. Somiya), MRS Symp. Proc. Series, Vol. 78, p. 75. Pittsburg, Pa (1987).
55. P. E. Reyes-Morel and I-W. Chen, *J. Am. Ceram. Soc.* **71,** 343 (1988).
56. J. W. Gibbs, On the equilibrium of heterogeneous substances, in *The Scientific Papers of J. W. Gibbs, V. 1 Thermodynamics*, p. 55. Dover, New York (1928).
57. J. M. Howe, in *Phase Transformations '87* (edited by G. W. Lorimer), p. 637. Inst. of Metals, London (1988).
58. H. L. Clark and C. M. Wayman, in *Phase Transformations* (edited by H. I. Aaronson), p. 59. Am. Soc. Metals, Metals Park, Ohio (1970).
59. A. L. Roitburd, *Soviet Phys. Usp.* **17,** 326 (1974).
60. A. G. Khachaturyan, *Theory of Structural Transformation in Solids.* Wiley-Interscience, New York (1983).
61. J. M. Howe, U. Dahman and R. Gronsky, *Phil. Mag. A* **56,** 31 (1987).